

Band gap narrowing in ferroelectric $\text{KNbO}_3\text{-Bi(Yb,Me)O}_3$ (Me=Fe or Mn) ceramics

Cristina Pascual-Gonzalez, Giorgio Schileo, and Antonio Feteira

Citation: *Appl. Phys. Lett.* **109**, 132902 (2016); doi: 10.1063/1.4963699

View online: <http://dx.doi.org/10.1063/1.4963699>

View Table of Contents: <http://aip.scitation.org/toc/apl/109/13>

Published by the [American Institute of Physics](#)

Articles you may be interested in

[Temperature stable and fatigue resistant lead-free ceramics for actuators](#)

Applied Physics Letters **109**, 142907 (2016); 10.1063/1.4964411

[Continuously controllable optical band gap in orthorhombic ferroelectric \$\text{KNbO}_3\text{-BiFeO}_3\$ ceramics](#)

Applied Physics Letters **110**, 172902 (2017); 10.1063/1.4982600

[Ferroelectric, pyroelectric, and piezoelectric properties of a photovoltaic perovskite oxide](#)

Applied Physics Letters **110**, 063903 (2017); 10.1063/1.4974735

[Weak-relaxor behaviour in Bi/Yb-doped \$\text{KNbO}_3\$ ceramics](#)

Applied Physics Letters **99**, 192901 (2011); 10.1063/1.3660255

[Structural phase transition, narrow band gap, and room-temperature ferromagnetism in \$\[\text{KNbO}_3\]_{1-x}\[\text{BaNi}_{1/2}\text{Nb}_{1/2}\text{O}_{3-\delta}\]_x\$ ferroelectrics](#)

Applied Physics Letters **105**, 111904 (2014); 10.1063/1.4896317

[Band gap engineering strategy via polarization rotation in perovskite ferroelectrics](#)

Applied Physics Letters **104**, 152903 (2014); 10.1063/1.4871707

Scilight

Sharp, quick summaries **illuminating**
the latest physics research

Sign up for **FREE!**

AIP
Publishing

Band gap narrowing in ferroelectric $\text{KNbO}_3\text{-Bi(Yb,Me)O}_3$ (Me=Fe or Mn) ceramics

Cristina Pascual-Gonzalez, Giorgio Schileo,^{a)} and Antonio Feteira

Christian Doppler Laboratory for Advanced Ferroics, Materials Engineering and Research Institute, Sheffield Hallam University, Howard Street, Sheffield S1 1WB, United Kingdom

(Received 1 August 2016; accepted 14 September 2016; published online 28 September 2016)

The direct optical bandgap in ferroelectric $\text{KNbO}_3\text{-Bi(Yb,Me)O}_3$ (Me = Fe or Mn) ceramics fabricated by the solid state reaction method varies from 3.2 eV for KNbO_3 down to 2.2 eV for $0.95\text{KNbO}_3\text{-}0.05\text{BiYbO}_3$, as revealed by optical spectroscopic ellipsometry. This narrowing of bandgap is accompanied by an apparent increase of the room-temperature relative permittivity from 320 for KNbO_3 to 900 for $0.95\text{KNbO}_3\text{-}0.05\text{BiYbO}_3$. All compositions studied exhibit dielectric anomalies associated with structural phase transitions, and their ferroelectric nature is corroborated by the presence of a sharp mixed mode (at $\sim 190\text{ cm}^{-1}$) and by a Fano-type resonant dip in their Raman spectra. *Published by AIP Publishing.* [<http://dx.doi.org/10.1063/1.4963699>]

Solar energy is one of the most promising sources of renewable, clean energy to replace our current dependence on fossil fuels. In conventional solid-state photovoltaics (for example, Si-based solar cells), electron-hole pairs are created by light absorption and then separated using the potential developed at a p-n junction or heterojunction. The maximum photovoltage in these devices is equal to the semiconductor electronic bandgap. In contrast, oxide ferroelectric (FE) perovskites (ABO_3) exhibit photovoltages exceeding several times their bandgap values.¹ This abnormal photovoltaic effect in FE has been known for more than 50 years. Nevertheless, it has been largely disregarded for technological applications because in most oxide FE perovskites, the optical bandgaps are usually greater than 3 eV, limiting their light absorption primarily to the ultraviolet (UV) region, i.e., they are only able to capture $\sim 8\%$ of the solar spectrum. The wide optical bandgaps in oxide FE perovskites arise from the nature of the bonding between O and B ions. Indeed, the large differences in electronegativity between the O and the B ions lead to the valence band to be formed by the 2p O states and the conduction band by the d states of the B transition metals sitting within the O octahedra. Until very recently, BiFeO_3 with a bandgap of 2.7 eV was known to have the narrowest bandgap among the oxide FE perovskites.² Nevertheless, BiFeO_3 is only able to capture 20% of the solar spectrum. BiFeO_3 thin films were observed to exhibit photovoltages that exceeded their bandgap by several times.³ The bulk nature of this phenomenon has been elegantly demonstrated by Bhatnagar *et al.*⁴ A comprehensive study on how the crystal and defect chemistry influences the bandgap trends in alkaline earth perovskites was carried out by Lee *et al.*⁵ They found the optical bandgap to vary systematically with tolerance factor and lattice volume within the limits defined by the chemistry of the octahedral site.

Recently, Grinberg *et al.*⁶ demonstrated that the direct bandgap of ferroelectric $(1-x)\text{KNbO}_3\text{-}x\text{BaNi}_{0.5}\text{Nb}_{0.5}\text{O}_{3-\delta}$ (KBNNO) ceramics can be tailored to values as low as

1.1 eV. Their first principle calculations have shown the valence band maximum to be composed of hybridized Ni 3d and O 2p states, while the conduction band minimum to be composed of Nb 4d states. Hence, they suggested that the filled Ni 3d gap states in the KBNNO ceramics play a crucial part in narrowing the bandgap. Bandgaps of vacancy-free $75\%\text{KNbO}_3\text{-}25\%(\text{Pb}_{0.5}\text{Bi}_{0.5})(\text{Zn}_{0.5}\text{Nb}_{0.5})\text{O}_3$ and $75\%\text{KNbO}_3\text{-}25\%(\text{Sr}_{0.5}\text{La}_{0.5})(\text{Zn}_{0.5}\text{Nb}_{0.5})\text{O}_3$ were predicted from first principle calculations as 2.92 eV and 2.11 eV, respectively.⁷ In this letter, we present the crystal structure, relative permittivity, and bandgap of KNbO_3 and self-compensated $95\%\text{KNbO}_3\text{-}5\%\text{BiYbO}_3$, $95\%\text{KNbO}_3\text{-}5\%\text{BiYb}_{0.5}\text{Fe}_{0.5}\text{O}_3$, and $95\%\text{KNbO}_3\text{-}5\%\text{BiYb}_{0.5}\text{Mn}_{0.5}\text{O}_3$ ceramics. In relation to undoped KNbO_3 with a bandgap of 3.2 eV, the narrower bandgap among the three doped compositions is 2.2 eV, and it is observed for $95\%\text{KNbO}_3\text{-}5\%\text{BiYbO}_3$. This result shows that the presence of transition metals is not a necessary condition to lower the bandgap. Moreover, it also shows the need to further understand bandgap engineering of ferroelectrics.

Dried K_2CO_3 (>99.0%), Nb_2O_5 (>99.9%, Aldrich), Bi_2O_3 (>99.9%, Aldrich), Yb_2O_3 (>99.9%, Aldrich), Fe_2O_3 (>99.0%, Aldrich), and MnO_2 (>99.9%, Aldrich) powders were weighed according to the KNbO_3 formula and self-compensated $95\%\text{KNbO}_3\text{-}5\%\text{BiYbO}_3$, $95\%\text{KNbO}_3\text{-}5\%\text{BiYb}_{0.5}\text{Fe}_{0.5}\text{O}_3$, and $95\%\text{KNbO}_3\text{-}5\%\text{BiYb}_{0.5}\text{Mn}_{0.5}\text{O}_3$ formulae. These powders were placed into a 250 ml milling polyethylene bottle together with ~ 0.5 kg of yttrium-stabilized zirconia milling media and ~ 100 ml of propan-2-ol samples and then mixed on a roller ball mill for ~ 20 h. Mixed powders were dried and then passed through a $500\ \mu\text{m}$ mesh sieve. The sieved powders were pressed into pellets and reacted between 500 and 1000°C with intermittent re-grinding and re-firing until no change on X-ray diffraction (XRD) data was visible. The fully reacted powders were pressed as 8 mm pellets and fired up to 1070°C for 2 h. The pellets were stacked on top of each other and sintered in a closed alumina crucible to limit loss of K and Bi. Purity and crystal structure analyses were carried out by XRD using a Bruker diffractometer (model D8) set up in transmission geometry and using monochromatic $\text{Cu K}\alpha_1$ radiation. The

^{a)}Now at Dyesol UK Ltd., UMIC, 48 Grafton Street, Manchester M13 9XX, United Kingdom.

XRD patterns were acquired in the 20–60 2θ range, with a step size of 0.02° with a scan length of 2 s per step. Raman spectra were obtained with a Renishaw Raman microscope (model InVia) using a 532 nm solid state (100 mW) laser, in back-scattering geometry using a 50 cm^{-1} edge filter. Temperature dependent Raman measurements were carried out using a Linkam (THMS600) Temperature Controlled Stage. Modes were assigned according to the literature data obtained from single crystals.⁸ Platinum electrodes were coated onto the faces of the sintered pellets for electrical measurements. Capacitance measurements were carried out with a Solartron impedance analyser (model 1260) coupled with a computer-controlled furnace. Finally, samples were finely polished with the colloidal silica for variable-angle spectroscopic ellipsometry measurements, which was carried out with a J. A. Woollam (model M2000) ellipsometer equipped with the Glan–Taylor polarizers, a rotating compensator, and deuterium and quartz halogen lamps for spectral coverage. Bandgaps were estimated from the average of three measurements at 40° , 55° , and 70° , and for each angle of incidence, at least two measurements were taken. Data were fitted using a blank model with a Tauc-Lorentz oscillator. Direct optical bandgaps were estimated by taking the zero-intercepts of the linear portion of the $(\alpha h\nu)^2$ vs $h\nu$ curves, where α and $h\nu$ are the absorption coefficient (in cm^{-1}) and the energy of the incident photon (in eV), respectively.⁶

Fig. 1 shows the room-temperature XRD data for KNbO_3 and self-compensated 95% KNbO_3 -5% BiYbO_3 , 95% KNbO_3 -5% $\text{BiYb}_{0.5}\text{Fe}_{0.5}\text{O}_3$, and 95% KNbO_3 -5% $\text{BiYb}_{0.5}\text{Mn}_{0.5}\text{O}_3$ ceramics. Within the detection limits of the technique, undoped KNbO_3 ceramics appear to be single-phase and the symmetry of their crystal structure to be well described by the orthorhombic $\text{Amm}2$ space group. Residual

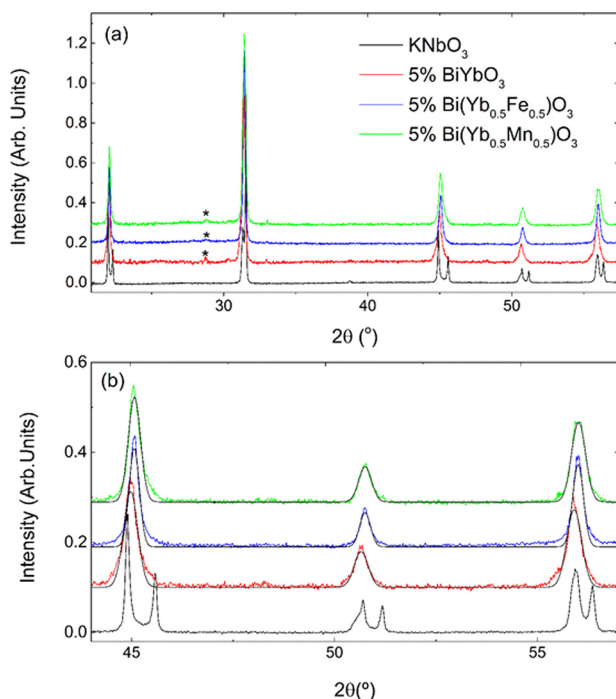


FIG. 1. Room-temperature XRD data in the (a) 20 to 60 (2θ) and (b) 44 to 58 (2θ) for KNbO_3 , 95% KNbO_3 -5% BiYbO_3 , 95% KNbO_3 -5% $\text{BiYb}_{0.5}\text{Fe}_{0.5}\text{O}_3$, and 95% KNbO_3 -5% $\text{BiYb}_{0.5}\text{Mn}_{0.5}\text{O}_3$ (from bottom to top). Asterisk indicates residual YbNbO_4 .

YbNbO_4 (ICDD card # 00-023-1480) is detected in all doped compositions, as indicated by asterisks in Fig. 1(a). Lattice parameters for KN ceramics were calculated as $a = 3.9728(1)\text{ \AA}$, $b = 5.6880(1)\text{ \AA}$, and $c = 5.7111(1)\text{ \AA}$, which are in broad agreement with the ICDD card # 00-032-0822. The XRD data for KN exhibits the typical peak splitting expected for a perovskite with orthorhombic crystal symmetry, but within the resolution of our measurements, only single peaks are visible for doped ceramics, as shown in Fig. 1(b). Nevertheless, those single peaks are asymmetric, indicating a clear lattice distortion away from the perfect cubic symmetry. A closer inspection of the shoulders suggests the doped ceramics to still show an average orthorhombic crystal symmetry. This is further corroborated by the room-temperature Raman spectroscopy data in Fig. 2. Indeed, the typical spectral features exhibited by orthorhombic KNbO_3 are also visible in the Raman spectra of all doped ceramics. Basically, this spectral similarity is sufficient to describe all ceramics in the orthorhombic $\text{Amm}2$ space group, as explained later in more detail. Finally, XRD reflections for doped compositions shift towards lower 2θ angles, indicating an increase in the unit cell volume. It follows that 95% KNbO_3 -5% BiYbO_3 possesses the largest unit cell. This corroborates the Yb^{3+} B-site occupancy, as this cation has a larger ionic radius in comparison with Nb^{5+} , Fe^{3+} and Mn^{3+} . Comprehensive studies of the KNbO_3 - BiYbO_3 and KNbO_3 - $\text{BiYb}_{0.5}\text{Fe}_{0.5}\text{O}_3$ systems will be presented elsewhere.

It can be anticipated that the simultaneous B-site occupancy by cations of very dissimilar ionic radius combined by the incorporation of Bi^{3+} in the A-site of the KNbO_3 lattice gives rise to local lattice distortions, which cannot be discerned from the XRD data. For example, in a previous letter,⁹ we have shown the XRD data for 80% KNbO_3 -20% BiYbO_3 to be described by the cubic centrosymmetric $\text{Pm}\bar{3}m$ space group; however, Raman spectroscopy revealed both the occurrence of local lattice distortions and the disruption of the long-range FE order. Hence, Raman spectroscopy analyses, Fig. 2, were employed to monitor the changes in the local structure and to ascertain the FE nature of the materials, as described below.

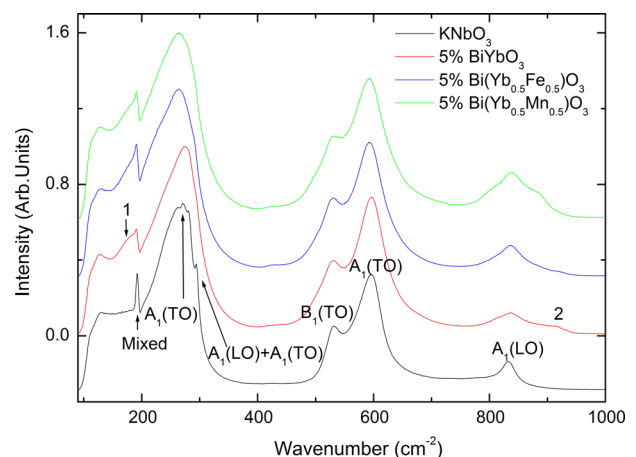


FIG. 2. Room-temperature Raman data for KNbO_3 , 95% KNbO_3 -5% BiYbO_3 , 95% KNbO_3 -5% $\text{BiYb}_{0.5}\text{Fe}_{0.5}\text{O}_3$, and 95% KNbO_3 -5% $\text{BiYb}_{0.5}\text{Mn}_{0.5}\text{O}_3$ (from bottom to top).

From group theory analysis, the following 12 optical modes are expected for point group $mm2$: $4A_1 + 4B_1 + 3B_2 + A_2$. All these modes are Raman active, but since in our experiment the Raman spectra are unpolarized, modes of all symmetry species are collected at the same time. Hence, fewer modes are observed due to the overlapping and mixing of the modes. Assignment of modes in the Raman spectrum of KNbO_3 was carried out according to the single-crystal assignment by Shen *et al.*⁸ Hence, in the low- to mid-wavenumber region, the Raman spectrum of KNbO_3 is characterised by (i) a broad A_1 (TO) mode centered at 270 cm^{-1} , which is assigned to BO_6 bending, (ii) a Fano-type interference dip at 195 cm^{-1} , and (iii) two sharp modes at 192 cm^{-1} and 296 cm^{-1} , respectively. Both (ii) and (iii) features are believed to be a fingerprint for the occurrence of long-range polar order in KNbO_3 . The sharp mode at 192 cm^{-1} is actually a mixed mode due to $B_1(\text{TO})$, $A_1(\text{TO})$, $A_1(\text{LO})$, and $B_2(\text{TO})$ modes, while the mode at 296 cm^{-1} is due to $A_1(\text{LO})$ and $A_1(\text{TO})$, but because of the resolution limit of the instrument, they appeared merged as a single peak. The high wavenumber region ($>500\text{ cm}^{-1}$) of the Raman spectrum of KNbO_3 is characterized by a $B_1(\text{TO})$ mode (at $\sim 532\text{ cm}^{-1}$), a $A_1(\text{TO})$ mode (at $\sim 596\text{ cm}^{-1}$), and a $A_1(\text{LO})$ (at 834 cm^{-1}) mode. Those are associated with vibrations of the octahedra. Upon doping, new modes emerge, which here have been numerically labelled as 1 and 2; because at this stage, information on their origin is merely speculative. The new mode 1 ($\sim 175\text{ cm}^{-1}$) appears as a shoulder to the sharp mixed mode at 192 cm^{-1} . This mode is fairly stationary as it only shifts by $\sim 2\text{ cm}^{-1}$ over the composition range $0 \leq x \leq 0.2$, as it will be shown elsewhere. In the past, this mode has been associated with A-O vibrations, in particular, to nm-sized clusters rich in either Bi^{3+} or K^+ cations. Mode 2 appears around $\sim 820\text{ cm}^{-1}$, and it has been previously associated with breathing of the octahedra, when occupied by different B cations.

In semiconductive FE materials, Raman spectroscopy analysis are more reliable to probe ferroelectricity than polarization, P , vs electric field, E , measurements. Indeed, often unsaturated PE loops can be observed for semiconductive non-FE materials. The two spectral features recognized as the fingerprint for long-range FE order in KNbO_3 are present in the Raman spectra of all doped compositions reported in this letter, as shown in Fig. 2. Nevertheless, it is worth to mention that those two features are absent from the spectra of $(1-x)\text{KNbO}_3-x\text{BiYbO}_3$ ceramics for $x \geq 0.10$, as it will be presented elsewhere. Hence, long-range polar order is absent in $(1-x)\text{KNbO}_3-x\text{BiYbO}_3$ ceramics for $x \geq 0.10$. In fact, we have previously shown that long-range polar order in KNbO_3 is replaced by short-range polar order in $(1-x)\text{KNbO}_3-x\text{BiYbO}_3$ ceramics for $x = 0.20$ and 0.30 .⁹ Those two compositions exhibit a so-called weak relaxor behaviour,⁹ which can be more specifically regarded as a re-entrant dipole glass behaviour.¹⁰

The temperature dependence of the relative permittivity for KNbO_3 and $95\%\text{KNbO}_3-5\%\text{BiYbO}_3$, $95\%\text{KNbO}_3-5\%\text{BiYb}_{0.5}\text{Fe}_{0.5}\text{O}_3$, and $95\%\text{KNbO}_3-5\%\text{BiYb}_{0.5}\text{Mn}_{0.5}\text{O}_3$ ceramics measured at 100 kHz is illustrated in Fig. 3. KNbO_3 shows two clear dielectric anomalies at $398\text{ }^\circ\text{C}$ and $223\text{ }^\circ\text{C}$, which can be ascribed to the cubic-to-tetragonal and to the tetragonal-to-

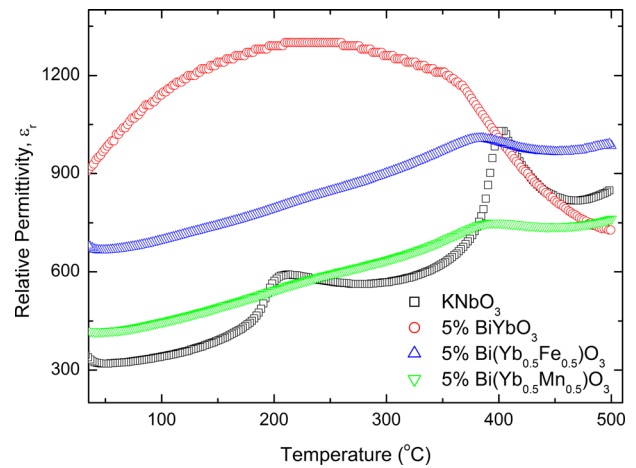


FIG. 3. Temperature dependence of the relative permittivity of KNbO_3 , $95\%\text{KNbO}_3-5\%\text{BiYb}_{0.5}\text{Mn}_{0.5}\text{O}_3$, $95\%\text{KNbO}_3-5\%\text{BiYb}_{0.5}\text{Fe}_{0.5}\text{O}_3$, and $95\%\text{KNbO}_3-5\%\text{BiYbO}_3$ (from bottom to top).

orthorhombic structural phase transitions. On the single-crystal, these transitions were reported to occur on heating at $420\text{ }^\circ\text{C}$ and $220\text{ }^\circ\text{C}$.¹¹ This difference may be caused by the impurities present in the starting raw materials, in particular, in K_2CO_3 , which has the lowest purity. In $95\%\text{KNbO}_3-5\%\text{BiYbO}_3$ ceramics, the tetragonal to cubic transition occurs at $353\text{ }^\circ\text{C}$; however, the maximum permittivity occurs at $231\text{ }^\circ\text{C}$. This composition shows the highest relative permittivity over the entire temperature range considered. $95\%\text{KNbO}_3-5\%\text{BiYb}_{0.5}\text{Fe}_{0.5}\text{O}_3$ and $95\%\text{KNbO}_3-5\%\text{BiYb}_{0.5}\text{Mn}_{0.5}\text{O}_3$ ceramics show similar behaviour; the only difference is the apparent larger permittivity of the Fe-based ceramics.

In order to further evaluate the evolution of structural phase transitions and to assert the presence of long-range polar order, *in-situ* Raman spectroscopy analyses were carried out in the temperature range of -180 to $280\text{ }^\circ\text{C}$. In Fig. 4, for the sake of simplicity, data are only presented for three different temperatures ($-180\text{ }^\circ\text{C}$, $120\text{ }^\circ\text{C}$, and $270\text{ }^\circ\text{C}$), which are representative of the three ferroelectric polymorphic structures exhibited by KNbO_3 . In Fig. 4(a), the spectra collected at $270\text{ }^\circ\text{C}$ are consistent with the ferroelectric tetragonal polymorph. On cooling, the clear separation of the $B_1(\text{TO})$ and $A_1(\text{TO})$ modes in the $500\text{--}650\text{ cm}^{-1}$ region is consistent with the ferroelectric orthorhombic polymorph, as shown in Fig. 4(b) for the data collected at $120\text{ }^\circ\text{C}$. Finally, at $-180\text{ }^\circ\text{C}$, spectra in the $150\text{--}300\text{ cm}^{-1}$ region show the spectral signature typical for the ferroelectric rhombohedral polymorph. It is noteworthy that the aforementioned modes 1 and 2 are present at all temperatures. Hence, based on both permittivity measurements and Raman spectroscopy analysis, all studied ceramics exhibit dielectric anomalies associated with structural phase transitions, and their ferroelectric nature is corroborated by the presence of a sharp mixed mode (at $\sim 190\text{ cm}^{-1}$) and by a Fano-type resonant dip in their Raman spectra. Basically, all studied ceramics are ferroelectric in a wide temperature range.

Finally, the compositional dependence of the bandgap values for KNbO_3 and self-compensated $95\%\text{KNbO}_3-5\%\text{BiYbO}_3$, $95\%\text{KNbO}_3-5\%\text{BiYb}_{0.5}\text{Fe}_{0.5}\text{O}_3$, and $95\%\text{KNbO}_3-5\%\text{BiYb}_{0.5}\text{Mn}_{0.5}\text{O}_3$ ceramics is listed in Table I.

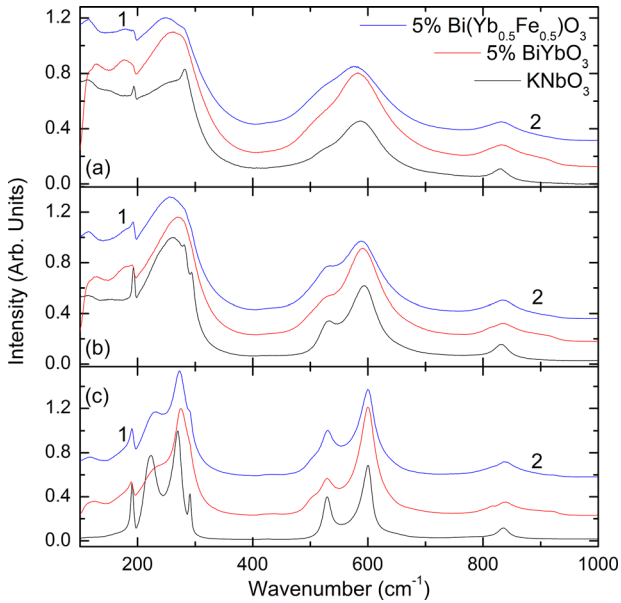


FIG. 4. Raman spectroscopy data at (a) 270 °C, (b) 120 °C and (c) -180 °C for KNbO₃, 95%KNbO₃-5%BiYbO₃, and 95%KNbO₃-5%BiYb_{0.5}Fe_{0.5}O₃. (From bottom to top).

These values were extrapolated from the Tauc's plot illustrated in Fig. 5. The direct bandgap for KNbO₃ is ~ 3.2 eV. This is very close to the values reported elsewhere.¹² The narrowest direct bandgap for the three doped compositions is 2.2 eV and is observed for 95%KNbO₃-5%BiYbO₃. This shows that the presence of transition metals is not a necessary condition to narrow the bandgap of KNbO₃. The general broadening of the Raman modes for doped ceramics, Fig. 4, results from the increased lattice disorder, which manifests itself by the emergence of Urbach tails in the Tauc plots, Fig. 5.

It is also worth to mention that the apparent increase of the relative permittivity, Fig. 3, appears to follow the narrowing of the bandgaps, Fig. 5. A correlation between the dielectric response and optical behavior of other KNbO₃-based solid solutions will be reported elsewhere.

Narrower bandgaps (as low as 1.1 eV) are achievable for (1-x)KNbO₃-xBaNi_{0.5}Nb_{0.5}O_{3- δ} (KBNNO) ceramics;⁶ however, oxygen vacancies may play a significant role on both the conduction and valence band energies, as postulated by Qi *et al.*,¹³ and in some cases, it may narrow the bandgap by ~ 0.5 eV. Unfortunately, the presence of oxygen vacancies is detrimental not only to polarization switching but can also trap the photogenerated carriers and increase the charge recombination rate as discussed by Wang *et al.*,⁷ who used first principle calculations to estimate the bandgaps for vacancy-free KNbO₃ co-doped with Zn and two different

TABLE I. Direct optical bandgaps.

Composition	Direct E _{gap} (eV)
KNbO ₃	3.2
95%KNbO ₃ -5%BiYbO ₃	2.2
95%KNbO ₃ -5%BiYb _{0.5} Fe _{0.5} O ₃	2.4
95%KNbO ₃ -5%BiYb _{0.5} Mn _{0.5} O ₃	2.6

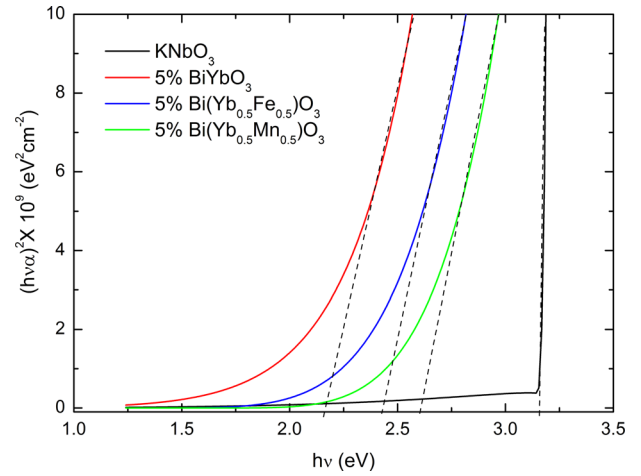


FIG. 5. Tauc plot for KNbO₃, 95%KNbO₃-5%BiYb_{0.5}Mn_{0.5}O₃, 95%KNbO₃-5%BiYb_{0.5}Fe_{0.5}O₃, and 95%KNbO₃-5%BiYbO₃ (from right to left).

A-sites ($A_1^{2+} = \text{Pb}^{2+}, \text{Ba}^{2+}, \text{Sr}^{2+}$ and $A_2^{3+} = \text{La}^{3+}, \text{Bi}^{3+}$) in order to achieve charge neutrality. The predicted bandgaps for those systems range between 2.92 eV and 2.11 eV. In our study, the experimental values of the optical bandgaps for self-compensated doped KNbO₃ lie broadly within this range as shown in Fig. 5 and Table I. The minute amount of YNbO₄ is unlikely to have any measurable impact on the dielectric properties and on bandgap narrowing.

In summary, it was demonstrated that the bandgap of KNbO₃ can be narrowed by 1 eV (i.e., a $\sim 30\%$ reduction) using dopants other than transition metals. Remarkably, bandgap narrowing was achieved while maintaining long-range polar order over a wide temperature range.

The XRD and the Raman Microscope used in this research were obtained through the Birmingham Science City: Creating and Characterizing Next Generation Advanced Materials (West Midlands Centre for Advanced Materials Project 1), with support Advantage West Midlands and partly funded by the European Regional Development Fund. Mr. L. Luisman is acknowledged for sample preparation and the performance of some measurements and Professor A. Nabok for sharing his expertise on ellipsometry. This work was partially supported by Christian Doppler Research Association in collaboration with EPCOS OHG (a TDK group company).

¹C. S. Tu, C. M. Hung, V. H. Schmidt, R. R. Chien, M. D. Jiang, and J. Anthoninappen, *J. Phys.: Condens. Matter* **24**(49), 495902 (2012).

²C. M. Hung, C. S. Tu, W. D. Yen, L. S. Jou, M. D. Jiang, and V. H. Schmidt, *J. Appl. Phys.* **111**(7), 07D912 (2012).

³R. K. Katiyar, Y. Sharma, P. Misra, V. S. Puli, S. Sahoo, A. Kumar, J. F. Scott, G. Morell, B. R. Weiner, and R. S. Katiyar, *Appl. Phys. Lett.* **105**(17), 172904 (2014).

⁴A. Bhatnagar, A. R. Chaudhuri, Y. H. Kim, D. Hesse, and M. Alexe, *Nat. Commun.* **4**, 2835 (2013).

⁵S. Lee, W. H. Woodford, and C. A. Randall, *Appl. Phys. Lett.* **92**(20), 201909 (2008).

⁶I. Grinberg, D. V. West, M. Torres, G. Y. Gou, D. M. Stein, L. Y. Wu, G. N. Chen, E. M. Gallo, A. R. Akbashev, P. K. Davies, J. E. Spanier, and A. M. Rappe, *Nature* **503**(7477), 509 (2013).

⁷F. G. Wang, I. Grinberg, and A. M. Rappe, *Phys. Rev. B* **89**(23), 235105 (2014).

- ⁸Z. X. Shen, Z. P. Hu, T. C. Chong, C. Y. Beh, S. H. Tang, and M. H. Kuok, *Phys. Rev. B* **52**(6), 3976 (1995).
- ⁹L. Luisman, A. Feteira, and K. Reichmann, *Appl. Phys. Lett.* **99**(19), 192901 (2011).
- ¹⁰V. Krayzman, I. Levin, J. C. Woicik, and F. Bridges, *Appl. Phys. Lett.* **107**(19), 192903 (2015).
- ¹¹G. Shirane, H. Danner, A. Pavlovic, and R. Pepinsky, *Phys. Rev.* **93**(4), 672 (1954).
- ¹²W. L. Zhou, H. M. Deng, P. X. Yang, and J. H. Chu, *Appl. Phys. Lett.* **105**(11), 111904 (2014).
- ¹³T. T. Qi, M. T. Curran, S. Kim, J. W. Bennett, I. Grinberg, and A. M. Rappe, *Phys. Rev. B* **84**(24), 245206 (2011).